Astronomy & Astrophysics manuscript no. exo4b
July 24, 2008

LETTER TO THE EDITOR

Transiting exoplanets from the CoRoT space mission

IV. CoRoT-Exo-4b: A transiting planet in a 9.2 day synchronous orbit⋆

S. Aigrain[1], A. Collier Cameron[2], M. Ollivier[3], F. Pont[1], L. Jorda[4], J. M. Almenara[5] R. Alonso[4], P. Barge[4], P. Bordé[3], F. Bouchy[6], H. Deeg[5], R. De la Reza[7], M. Deleuil[4], R. Dvorak[8], A. Erikson[9], M. Fridlund[10], P. Gondoin[10], M. Gillon[11], T. Guillot[12], A. Hatzes[13], H. Lammer[14], A. F. Lanza[15] A. Léger[3], A. Llebaria[4], P. Magain[16], T. Mazeh[17], C. Moutou[4], M. Paetzold[18], C. Pinte[1], D. Queloz[11], H. Rauer[9,19], D. Rouan[20], J. Schneider[21], G. Wuchter[13], and S. Zucker[22]

(Affiliations can be found after the references)

Received . . . ; accepted . . .

ABSTRACT

CoRoT, the first space-based transit search, provides ultra-high precision light curves with continuous time-sampling over periods of up to 5 months. This allows the detection of transiting planets with relatively long periods, and the simultaneous study of the host star's photometric variability. In this letter, we report on the discovery of the transiting giant planet CoRoT-Exo-4b and use the CoRoT light curve to perform a detailed analysis of the transit and to determine the stellar rotation period. The CoRoT light curve was pre-processed to remove outliers and correct for orbital residuals and artefacts due to hot pixels on the detector. After removing stellar variability around each transit, the transit light curve was analysed to determine the transit parameters. A discrete auto-correlation function method was used to derive the rotation period of the star from the out-of-transit light curve. We derive periods for the planet's orbit and star's rotation of 9.20205 ± 0.00037 and 8.87 ± 1.12 days respectively, consistent with a synchronised system. We also derive the inclination, $i = 90.00^{+0.000}_{-0.085}$ in degrees, the ratio of the orbital distance to the stellar radius, $a/R_s = 17.36^{+0.05}_{-0.25}$, and the planet to star radius ratio $R_p/R_s = 0.1047^{+0.0041}_{-0.0022}$. We discuss briefly the coincidence between the orbital period of the planet and the stellar rotation period and its possible implications for the system's migration and star-planet interaction history.

Key words. planetary systems – techniques: photometry

1. Introduction

Transits provide unique insights into fundamental aspects of extra-solar planets that are currently beyond the reach of other techniques: mean density (through the determination of true masses and radii), atmospheres (through transmission spectroscopy and secondary transit observations), and formation and evolution mechanisms (through the statistics of the orbital parameters, including the true mass). All but two of the transiting planets published so far have been very short-period planets (< 5 d), whose properties are bound to be affected by extreme proximity to their host star. The exceptions are HD 147506b (Bakos et al. 2007) and HD 17156b (Barbieri et al. 2007), with periods of 5.6 and 21.2 d, both in very eccentric orbits ($e \geq 0.5$).

CoRoT is the first space-based transit survey, and over its lifetime will survey 120 000 stars for up to 5 months with precisions down to 0.1 mmag per hour. This letter is the 4th in a series presenting new extra-solar planets discovered thanks to the CoRoT observations and associated ground-based follow-up program. Papers I (Barge et al. 2008) and II (Alonso et al. 2008) present the discoveries of CoRoT-Exo-1b and CoRoT-Exo-2b, both very close-in giant planets. Paper III (Bouchy et al. 2008) reports on the observation of the spectroscopic transit of CoRoT-Exo-2b. Here we report on the detection of CoRoT-Exo-4b, a relatively long period (9.2 d) gas-giant transiting planet, and on the analysis of the CoRoT light curve (the production of which is described in Section 2) to determine the transit parameters (see Section 3) and the stellar rotation period (see Section 4). This analysis makes no assumptions aside from the planetary nature of the companion, which was confirmed through ground-based follow-up observations which are reported in a companion letter (Moutou et al. 2008 hereafter Paper V). In Paper V, the full system parameters are determined using the transit parameters reported in the present work. These parameters are used in Section 5, where we discuss the implications of the relatively long period and of its proximity to the stellar rotation period. A further detection, CoRoT-Exo-3b, will be presented in Deleuil et al. (2008, Paper VI).

2. Observations and data processing

Like the previously published CoRoT planets, CoRoT-Exo-4b was first detected during near real-time analysis of raw data, the 'alarm mode' (which is described in Papers I and II), triggering the ground-based follow-up described in Paper V, which included ground-based photometry in- and out-of-transit, at higher spatial resolution than CoRoT's own, to identify which of the stars falling in the CoRoT aperture was being eclipsed, and multiple radial velocity measurements to derive the companion mass. Once the planetary nature of the companion was confirmed, a high resolution, high signal-to-noise spectrum of the host star was obtained to derive accurate stellar parameters.

⋆ The CoRoT space mission, launched on December 27th 2006, has been developed and is operated by CNES, with the contribution of Austria, Belgium, Brasil, ESA, Germany and Spain. The first CoRoT data will be available to the public from February 2009 through the CoRoT archive: `http://idoc-corot.ias.u-psud.fr/`.

CoRoT-Exo-4 (GSC designation 0480002187), whose coordinates and magnitude are given in Table 1, was observed as part of CoRoT's initial run, during which ~ 12 000 stars with magnitude $12 < R < 16$ falling in a $1.3° \times 2.6°$ pointing close to the anticentre of the Galaxy were monitored nearly continuously for 58 days, starting on the 6th of February 2007. A total of 72319 flux measurements were obtained for CoRoT-Exo-4. For the first 33 d of the run, the time sampling is 512 s, after which it was switched to 32 s as the transits were detected by the alarm mode.

Aperture photometry through a mask, automatically selected from a set of 256 templates at the beginning of the run, is performed on board. For stars brighter than $R = 15$, the flux is split along detector column boundaries into broad-band red, green and blue channels. Although the transits were detected in the raw data, the analysis presented here was based on the pipeline-processed light curve. The pipeline (Auvergne et al. 2008) currently includes background subtraction and partial jitter correction. For each exposure, a global background level is estimated from a handful of 10×10 pixel background windows distributed over each CCD, excluding background windows affected by hot pixels, and subtracted. The jitter correction is based on the satellite line of sight information, which is derived from the asteroseismology channel (which lies next to the exoplanet channel on the focal plane). Currently, the pipeline only applies a relative jitter correction for the three colour channels. This correction conserves the total (white) flux, and no jitter correction for the total flux is attempted. The pipeline also flags data points collected during the SAA or affected by other events likely to impair the data quality, such as entrance into and exit from the Earth's shadow.

The blue channel light curve is affected by a hot pixel event a few days after the start of the observations, causing a sudden rise in the measured flux followed by a gradual decay of ~ 5 days. This was corrected by fitting an exponential curve to the decaying segment, excluding a small portion that falls in-transit (see Figure 1, online only). That section of the blue channel light curve also shows a gradual rise in flux. To preserve it, a linear rise between the local mean flux levels before and after the section of light curve affected by the hot pixel was added after subtracting the exponential decay. The red and green channels are free of visible hot pixel events. Note that the transit depth is the same in all three channels (within the uncertainties), as expected for a planetary transit.

A single band-pass is sufficient for the present work, so the flux from the three colour channels was summed to give a 'white' light curve (approximately covering the range 300–1000 nm). The three-colour photometry will be discussed in an upcoming paper pending improvements in the pipeline. Additionally, a version of the light curve with regular 512 s time sampling was computed by rebinning there over-sampled part of the original. This version was used to study the out-of-transit variability, while the over-sampled version was retained to estimate the transit parameters. A short-baseline (5 data points) iterative non-linear filter (Aigrain & Irwin 2004) with 5-σ clipping was applied to both the over-sampled and regularly sampled light curves to identify and reject further outliers, resulting in a final duty cycle of 87%.

Based on preliminary ground-based imaging of the field (Deleuil et al. 2006) and a basic empirical model of the CoRoT PSF, we estimate the contamination of the photometric aperture by other stars than CoRoT-Exo-4 to be 0.3 ± 0.1% (the uncertainty arises from the PSF model). This estimate is compatible with the transit depths measured from the ground (see Paper V). We therefore subtracted a constant equal to 0.3% of the median flux value, before normalising the light curve (the uncertainty is accounted for separately, see Section 3). The full normalised light curve is shown in Figure 2. We evaluate the actual noise level per 512 s by measuring the dispersion about 1 h (7 exposures) bins and scaling it by $\sqrt{7}$, giving 8.9×10^{-4}, compared to a photon noise level of 5.6×10^{-4}. Possible factors contributing to the difference include residual instrumental effects and the intrinsic variability of the star.

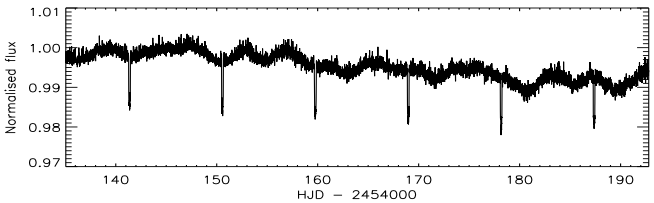

Fig. 2. Pre-processed white light curve of CoRoT-Exo-4. The light curve was normalised by dividing it by its own median, which gives more weight to the later (oversampled) part of the light curve. This does not affect the transit analysis, since it is the local out-of-transit flux around each transit that is taken as a reference (see Section 3).

Table 1. Star and transit parameters derived from the CoRoT light curve. The quantity $M_s^{1/3}/R_s$, which is used in determining the stellar parameters (see Paper V), is derived directly from a/R_S and P.

Parameter	Value	Bayesian range
RA	06 48 46.70	
Dec	−00 40 21.97	
R − mag	13.45	
P_{rot} (d)	8.87 ± 1.12	
P (d)	9.20205 ± 0.00037	
T_0 (HJD)	$2454141.36416 \pm 0.00089$	
i (°)	$90.000^{+0.000}_{-0.085}$	87.708 – 90.000
a/R_s	$17.36^{+0.05}_{-0.25}$	14.30 – 17.80
u	$0.44^{+0.16}_{-0.15}$	0.00 – 1.00
R_p/R_s	$0.1047^{+0.0041}_{-0.0022}$	0.1000 – 0.1125
$M_s^{1/3}/R_s$	$0.899^{+0.003}_{-0.013}$	0.741 – 0.922

3. Transit analysis

A preliminary ephemeris (orbital period P and epoch T_0) was obtained by least-squares fitting of periodic, trapezoidal transits to the light curve after filtering out the out-of-transit variations using a 1-day baseline iterative non-linear filter. A more careful removal of the variability was then carried out by fitting a straight line to a light curve section lasting a little over one transit duration before and after each transit. We also experimented with higher order polynomials, but they did not improve the dispersion of the residuals, and do not change the results of the subsequent analysis. We folded the corrected segments of light curve using the preliminary period ephemeris, rebinned them in bins of 0.0003 in phase, and fitted the result to obtain preliminary estimates of the system scale a/R_s, the radius ratio R_p/R_s, the inclination i and the linear limb-darkening coefficient u, where R_s is the star radius, R_p the planet radius and a the semi-major axis.

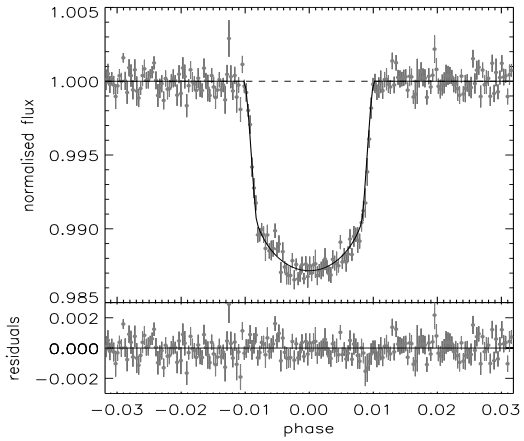

Fig. 3. Folded, binned light curve with the best-fit transit model.

We opted to fit for u rather than fix it because reliable theoretical limb-darkening coefficients are not currently available for the CoRoT bandpass. The ephemeris was then refined by fitting for the time of transit centre T_C for each individual transit event (fixing all other parameters) and fitting a linear relation to the T_C's. Finally, the light curve was folded again at the refined ephemeris and rebinned to perform a final fit for a/R_s, R_p/R_s, i and u.

At each stage, we use the formalism of Mandel & Agol (2002) with quadratic limb darkening to generate model transit light curves and the IDL implementation MPFIT of the Levenberg-Marquart fitting algorithm, kindly provided by C. Markwart, to perform the fit. The period was fixed at the ephemeris value, and the epoch was also fixed except when fitting individual transits. The eccentricity was assumed to be zero (the best fit to the radial velocity data is a circular orbit with an eccentricity uncertainty of 0.1, see Paper V). We also tried fitting the transits with a quadratic limb-darkening prescription, but this did not improve the fit, and therefore we reverted to linear limb-darkening.

To evaluate the noise-induced uncertainties on the transit parameters, including the effect of red noise, we used a 'correlated bootstrap' approach. The residuals from the global best fit were divided into bins lasting 1.12 h (2/3 of the transit duration, or 1/4 of the duration of the light curve segments used to calibrate the out-of-transit variations around each transit), randomly shuffled, and added back to the fit before fitting the individual transits. Over-sampled and non over-sampled bins were shuffled separately. Each bin is shuffled whole, preserving the detailed time sampling of individual bins, so the procedure does not account for the effect of small data gaps, but it does account for correlated noise on hour timescales, including the effect of star spots crossed by the planet. We used 100 realisations when fitting individual transits and 1000 when fitting the folded light curve. At each realisation, we also added a constant drawn from a Gaussian distribution with zero mean and standard deviation 0.001 to the data, to account for the uncertainty in the contamination fraction. As the frequency distributions for each parameter can be strongly non-Gaussian (see in Fig. 4 in the online material), we measure uncertainties as the interval away from the best-fit value where the frequency drops below $e^{-1/2}$ times the maximum (if the distributions were Gaussian, this would be equivalent to the standard deviation). The results are reported in Table 1. For comparison, we also show in Fig. 4 the results of a standard bootstrap (which simply consists in swapping data points, and accounts for white noise only). Except for the limb-darkening coefficient, the two processes give similar results, indicating that red noise affects the other parameters' only slightly.

To gain an insight into the effect of parameter-to-parameter correlations, we used a Bayesian approach. Reduced χ^2 values were computed over a grid in 4-dimensional parameter space (i, a/R_s, R_p/R_s and u) about the best fit. A uniform grid in $\cos(i)$ was used, which is equivalent to assuming an isotropic distribution of inclinations. The grid was uniform in the other parameters, i.e. no a priori information on these parameters was assumed (though u was restricted to the physical range 0–1). The χ^2's were then converted to relative probabilities for each individual model using $p \propto \exp(-\chi^2/2)$ and normalised. One can then obtain probability distributions for each parameter (shown on Fig. 4) by marginalising over successive parameters. For each parameter, we report in Table 1 the interval over which the probability is higher than $e^{-1/2}$ times the maximum. This interval should be interpreted with some care: it is not a confidence interval in the frequentist sense, but rather an interval containing $\sim 68\%$ of the posterior probability *integrated over all other parameters*[1]. In the present case, this interval is very wide because the global minimum in the multi-dimensional χ^2 surface is very narrow, but it is located at one end of a valley which widens significantly away from the minimum, as illustrated in Fig. 4.

In Paper V, the transit parameters are combined with ground-based follow-up observations to give the stellar and planetary parameters, which we reproduce here for completeness: $T_{\rm eff} = 6190 \pm 60$ K, $\log g = 4.41 \pm 0.05$, $M_s = 1.16^{+0.03}_{-0.02}\,M_\odot$, $R_s = 1.17^{+0.01}_{-0.03}\,R_\odot$, age $1^{+1.0}_{-0.3}$ Gyr; $M_p = 0.72 \pm 0.08\,M_{\rm Jup}$ and $R_p = 1.19^{+006}_{-0.05}\,R_{\rm Jup}$. Note that Claret (2004) compute theoretical linear limb-darkening coefficients in the range 0.55–0.6 for $T_{\rm eff} = 6250$ K and $\log g = 4.5$ in r', which is the standard bandpass closest to the peak of the CoRoT bandpass, though the later is much broader (300–1000 nm). This is compatible with the value of 0.44 ± 0.15 obtained from the transit fit.

We checked for transit timing variations in the $O - C$ (observed minus computed) residuals from the refined ephemeris. The results are given in Figure 5 (online only). The third transit in the time series shows a strong (> 500 s) deviation. To test whether this is a real timing variation, we repeated the individual transit fits allowing a/R_s and R_p/R_s to vary as well as T_C, and found a clear correlations between the timing residuals and a/R_s (see bottom left panel of Figure 5), which points towards the effect of star spots or instrumental systematics rather than a real timing variation as the cause of the outlier. Closer inspection reveals that this transit contains small data gaps, and we interpret the deviation in measured timing and duration as an artefact of these gaps rather than a physical effect. We also checked for a secondary eclipse (removing the variability around phase 0.5 using linear fits as done for the transits) but none is detected (as expected for this relatively low irradiation planet).

4. Stellar rotation

The light curve in Fig. 2 shows clear out-of-transit variability typical of a rotating, spotted photosphere. The semi-coherent nature of the light curve suggests that active regions on the star are evolving on timescales slightly longer than the rotation period. A given active region may therefore cross the visible hemisphere only 2 or 3 times in its lifetime. The form of the light curve evolves quickly, but partial coherency should persist for 2 or 3 rotations, making auto-correlation an appropriate method

[1] For an excellent discussion of Bayesian inference and model selection and how it differs from frequentist methods, see Trotta (2008).

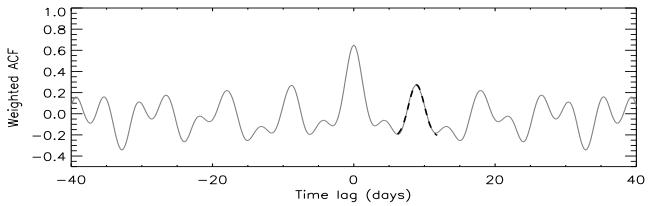

Fig. 6. Weighted auto-correlation function of the out-of-transit light curve (gray line). We estimate the rotation period of the star using a Gaussian fit to the peak of the first side-lobe (dashed black line).

to measure the stellar rotation period. We used an inverse variance weighted adaptation of the Discrete Correlation Function method of Edelson & Krolik (1988) (Collier Cameron et al. 2008) to compute the Auto-Correlation Function, or ACF (see Fig. 6). We fit a Gaussian to the first peak in the ACF to deduce a period of $P_{\rm ACF} = 8.87 \pm 1.12$ d. The dominant source of uncertainty is the limited duration of the time-series. This is consistent with the $v \sin i$ of 6.4 ± 1.0 km/s reported in Paper V.

5. Conclusions

CoRoT-Exo-4b's orbital period is the second longest of any transiting planet to date, following HD 17156b (Barbieri et al. 2007). To our knowledge, it is only the second transiting system where the star's photometric rotation period has been measured photometrically (the other being HD 189733, Henry & Winn 2008). There are other systems where the rotation period and planet orbital period are very similar, particularly τ Boo (Catala et al. 2007; Donati et al. 2008) and XO-3 (Johns-Krull et al. 2008; Winn et al. 2008) (the rotation periods are derived from Doppler imaging and $v \sin i$ respectively, rather than measured photometrically). In both cases, the period of the orbit and the stellar rotation period are not exactly the same, but is compatible with a synchronised outer envelope when allowing for differential surface rotation. Both planets, which orbit F-type stars like CoRoT-Exo-4, are massive and have very short periods (~ 3 d), and thus may induce strong enough tides in the star to have synchronised its convective envelope.

A simple calculation, based on the work of Dobbs-Dixon et al. (2004) and Jackson et al. (2008), shows that CoRoT-Exo-4b, which has a smaller mass and longer period, would not exert a significant tidal torque on its host star unless one invokes an unphysically high rate of tidal energy dissipation in the star. However, McCullough et al. (2008) discuss the case of two other transiting systems containing F-type stars, XO-4 and HAT-P-6, both with orbital periods longer than 7 days which are roughly half the (spectroscopically determined) stellar rotation period. They argue that this may indicate the existence of resonant interactions between the planet's orbit and its rotating host star, the absence of such resonances in systems containing cooler stars suggesting that Jupiter-mass planets can only interact effectively with stars with very shallow outer convective zones.

Similarly, if some other factor brought the CoRoT-Exo-4 system to the 1:1 ratio between stellar rotation and orbital period that is observed today, resonant interaction between star and planet may have maintained this ratio thereafter. Any subsequent evolution of the star's rotation rate is likely to have been modest: 9 d is close to the peak of the rotation period distribution for F-type stars both during the TTauri phase and in the field (see e.g. Fig. 1 of Barnes 2003). The initial resonance may have occured naturally if the proto-planetary disk was truncated near the co-rotation radius, and the planets' migration halted close to the inner edge of the disk. This hypothesis is supported by the absence of detectable eccentricity (see Paper V).

This system clearly warrants further observational and theoretical investigation to pin down its tidal and rotational evolution status. For example, more detailed analysis of the out-of-transit light curve should enable the active regions on the stellar surface to be mapped in a time-resolved fashion (Lanza et al. 2007) to search for signs of star-planet magnetic interaction.

Acknowledgements. HD and JMA acknowledge support from grant ESP2007-65480-C02-02 of the Spanish Science and Innovation ministry, the German CoRoT team (TLS and Univ. Cologne) from DLR grants 50OW0204, 50OW0603, and 50QP0701, AL from contract ASI/INAF I/015/07/0 (work package 3170), and SZ from the Israel Science Foundation – Adler Foundation for Space Research (grant no. 119/07).

References

Aigrain, S. & Irwin, M. 2004, MNRAS, 350, 335
Alonso, R., Auvergne, M., Baglin, A., et al. 2008, A&A, 482, L21
Auvergne, M., Bodin, P., Boisnard, L., et al. 2008, A&A, submitted
Bakos, G. Á., Kovács, G., Torres, G., et al. 2007, ApJ, 670, 826
Barbieri, M., Alonso, R., Laughlin, G., et al. 2007, A&A, 476, L13
Barge, P., Baglin, A., Auvergne, M., et al. 2008, A&A, 482, L17
Barnes, S. A. 2003, ApJ, 586, 464
Bouchy, F., Queloz, D., Deleuil, M., et al. 2008, A&A, 482, L25
Catala, C., Donati, J.-F., Shkolnik, E., Bohlender, D., & Alecian, E. 2007, MNRAS, 374, L42
Claret, A. 2004, A&A, 428, 1001
Collier Cameron, A., Davidson, V. A., Skinner, G., et al. 2008, MNRAS, submitted
Deleuil, M., Deeg, H., Alonso, R., et al. 2008, A&A, submitted
Deleuil, M., Moutou, C., Deeg, H. J., et al. 2006, in ESA SP-1306: The CoRoT mission: pre-launch status, ed. M. Fridlund, A. Baglin, L. Conroy, & J. Lochard (Noordwijk: ESA), 341–352
Dobbs-Dixon, I., Lin, D. N. C., & Mardling, R. A. 2004, ApJ, 610, 464
Donati, J.-F., Moutou, C., Farès, R., et al. 2008, MNRAS, 385, 1179
Edelson, R. A. & Krolik, J. H. 1988, ApJ, 333, 646
Henry, G. W. & Winn, J. N. 2008, AJ, 135, 68
Jackson, B., Greenberg, R., & Barnes, R. 2008, ApJ, 678, 1396
Johns-Krull, C. M., McCullough, P. R., Burke, C. J., et al. 2008, ApJ, 677, 657
Lanza, A. F., Bonomo, A. S., & Rodonò, M. 2007, A&A, 464, 741
Mandel, K. & Agol, E. 2002, ApJL, 580, L171
McCullough, P. R., Burke, C. J., Valenti, J. A., et al. 2008, ApJ, submitted, arXiV:0805.2921
Moutou, C., Bruntt, C., Guillot, T., et al. 2008, A&A, in press
Trotta, R. 2008, Contemporary Physics, in press
Winn, J. N., Holman, M. J., Torres, G., et al. 2008, ApJ, submitted, arXiV:0804.4475

[1] School of Physics, University of Exeter, Exeter, EX4 4QL, UK
[2] Sch. Physics & Astronomy, Univ. St Andrews, St Andrews KY16 9SS, UK
[3] IAS, Université Paris XI, 91405 Orsay, France
[4] LAM, Université de Provence, 13388 Marseille, France
[5] IAC, E-38205 La Laguna, Spain
[6] IAP, Université Pierre & Marie Curie, 75014 Paris, France
[7] ON/MCT, 20921-030, Rio de Janeiro, Brazil
[8] IfA, University of Vienna, 1180 Vienna, Austria
[9] Institute of Planetary Research, DLR, 12489 Berlin, Germany
[10] RSSD, ESA/ESTEC, 2200 Noordwijk, The Netherlands
[11] Observatoire de Genève, 1290 Sauverny, Switzerland
[12] OCA, CNRS UMR 6202, BP 4229, 06304 Nice Cedex 4, France
[13] Thüringer Landessternwarte, 07778 Tautenburg, Germany
[14] IWF, Austrian Academy of Sciences, A-8042 Graz, Austria
[15] INAF – Osservatorio Astrofisico di Catania, 95123 Catania, Italy
[16] IAG, Université de Liège, Liège 1, Belgium
[17] Sch. Physics & Astronomy, Tel Aviv Univ., Tel Aviv 69978, Israel
[18] RIU, Universität zu Köln, 50931 Köln, Germany
[19] ZAA, TU Berlin, D-10623 Berlin, Germany

[20] LESIA, Observatoire de Paris, 92195 Meudon, France
[21] LUTH, Observatoire de Paris, 92195 Meudon, France
[22] Dept. Geophysics & Planetary Sciences, Tel Aviv Univ., Tel Aviv 69978, Israel

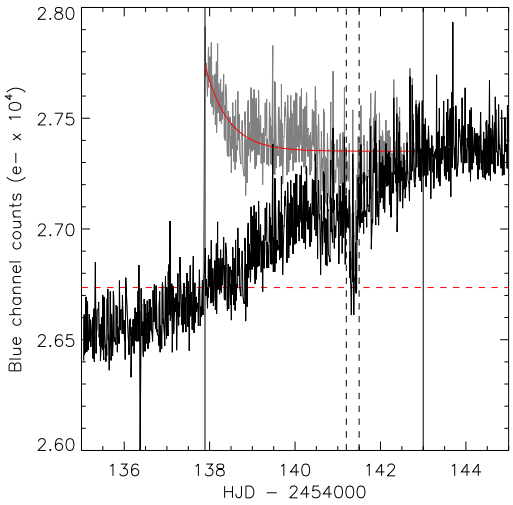

Fig. 1. Correction of the hot pixel event in the blue channel. The light curve before correction is shown in grey, and after correction in black. The vertical solid lines show the time limits of the correction section, with the exponential decay fit shown as the smooth red line. A small subsection, between vertical dashed lines, falls in-transit, and was not used to estimate the correction, though the correction was applied to it. The horizontal dashed line shows the reference flux level adopted before the hot pixel event.

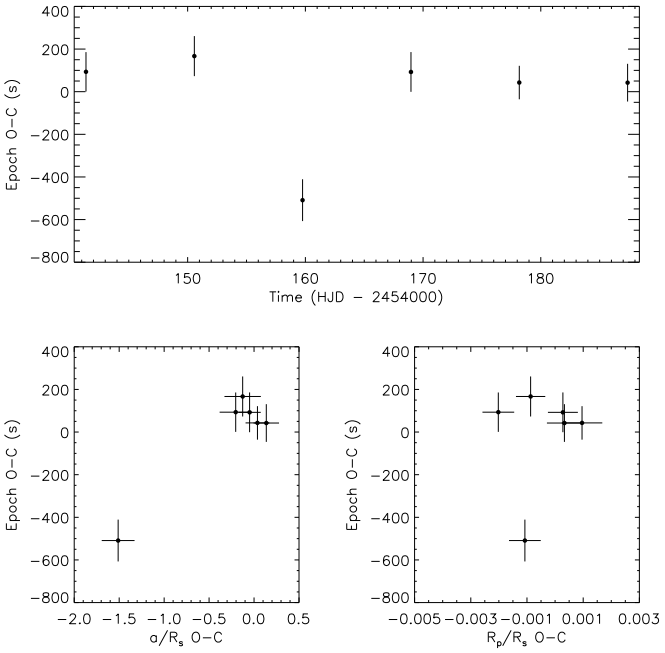

Fig. 5. Transit timing residuals versus time (top panel) and compared to variations in transit duration (measured through the scale parameter a/R_s) and depth (measured through the radius ratio R_p/R_s. The apparent timing deviation of the third transit is accompanied by a change in duration, but not in depth. Closer inspection of the light curve shows that this transit is more strongly affected by data gaps than the others.

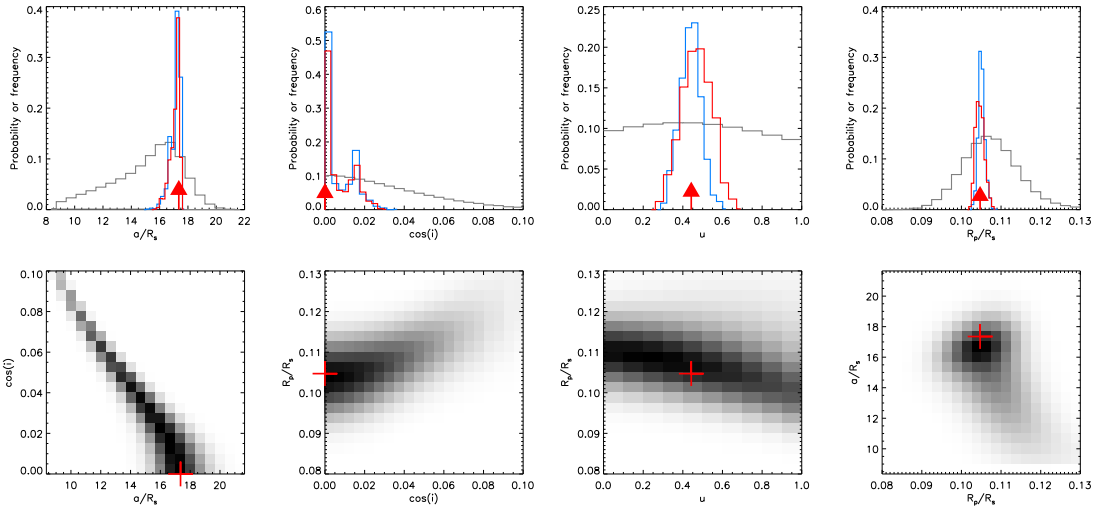

Fig. 4. Top: probability and frequency distributions obtained from the Bayesian and bootstrap methods respectively for the main parameters, a/R_s, $cos(i)$, u and R_p/R_s of the transit fit. The Bayesian method results are shown in grey, the correlated bootstrap in red and the non-correlated bootstrap in blue. Bottom: Two-dimensional probability distributions obtained from the Bayesian method for selected pairs of parameters, highlighting the correlations between parameters (particularly a/R_s and i). In each panel, the location of the best-fit model is marked by a red vertical arrow or cross.